Title: Alpha-synuclein expression supports interferon stimulated gene expression in neurons

Authors: Aaron R. Massey[1,6,8], Brendan Monogue[2,8], Yixi Chen[4], Kelsey Lesteberg[1], Michaela E. Johnson[5], Liza Bergkvist[5], Jennifer A. Steiner[5], Jiyan Ma[5], Ravi Mahalingam[3], Bette K. Kleinschmidt-Demasters[7], Martha Escobar Galvis[5], Patrik Brundin[5], Tilo Kunath[4], J. David Beckham[1,2,3,6*]

Affiliations:
[1] Division of Infectious Diseases, Department of Medicine, University of Colorado Anschutz Medical Campus, Aurora, CO.
[2] Department of Immunology&Microbiology, University of Colorado Anschutz Medical Campus, Aurora, CO.
[3] Department of Neurology, University of Colorado Anschutz Medical Campus, Aurora, CO.
[4] MRC Centre for Regenerative Medicine, School of Biological Sciences, and the UK Centre for Mammalian Synthetic Biology, University of Edinburgh, Edinburgh, UK
[5] Center for Neurodegenerartive Science, Van Andel Institute, Grand Rapids, MI
[6] Rocky Mountain Regional VA Medical Center, Aurora, CO
[7] Department of Pathology, University of Colorado Anschutz Medical Campus, Aurora, CO.
[8] These authors contributed equally.
*e-mail:David.beckham@cuanschutz.edu

Abstract:

The protein alpha-synuclein (asyn) is predominantly expressed in neurons and is associated with neurodegenerative diseases like Parkinson's disease (PD); yet, a functional role for asyn in neurons is not clearly established. We have previously shown that asyn expression is up-regulated following viral infection in neurons and may plays a key role in host immune responses to viral infections. Here we systematically characterize a functional role of asyn in the brain and in individual cells in brain tissue. We now show that asyn expression in the brain supports expression of specific interferon-stimulated genes (ISGs) following acute RNA virus infection in neurons. Using pluripotent stem cell-derived human neurons, we show that asyn mediates expression of ISGs following RNA virus infection and following treatment with poly

I:C and type 1 interferon. Our results establish a novel functional role for asyn in neuronal innate immunity by a mechanism that promotes interferon-stimulated gene expression.

One Sentence Summary: Alpha-synuclein modulates interferon stimulated gene expression in neurons.

Report

We evaluated the role of alpha-synuclein (asyn) in innate immunity based on previous findings showing that asyn is up-regulated in neurons following viral infection and that knockout of the asyn gene, *Snca*, in mice results in increased viral growth in the brain and increased mortality.(*1-3*) We previously reported that asyn knockout (KO) mice (*Snca* -/-) exhibit increased disease severity and viral growth in the brain following peripheral challenge with RNA viruses including West Nile virus (WNV) and Venezuelan equine encephalitis virus (VEEV) TC83.(*2*) An important subsequent study demonstrated that total asyn expression was elevated in gastrointestinal-associated neurons following viral gastroenteritis in children.(*3*) The same study also suggested that asyn expression supported chemotaxis and activation of infiltrating dendritic cells.(*3*) Most recently, intranasal inoculation of Western equine encephalitis virus (WEEV) was shown to result in viral spread along olfactory neuronal pathways of mice, resulting in activation of microglia and astrocytes in multiple brain regions, including the midbrain and striatum.(*1*) WEEV infection also resulted in prominent proteinase K-resistant aggregates of post-translationally modified asyn and loss of dopaminergic neurons in the substantia nigra.(*1*) Taken together, acute RNA virus infection increases asyn levels, asyn phosphorylation on serine residue 129, aggregation of asyn, and results in loss of nigral dopamine neurons; thereby recapitulating multiple key neuropathological features of PD. Despite these important recent findings, the specific role of asyn during acute viral infection remains unknown.

We aimed to define a functional role for asyn expression during acute viral infection. We first determined if asyn interacts in a species-specific role with conserved host factors during acute infection. To evaluate species-specific interactions, we used trans-complementation of human *SNCA* in the murine *Snca(-/-)* knockout (KO) model. Murine asyn KO mice that express the human *SNCA* from a P1 artificial chromosome (Tg*SNCA*(+/+) *Snca*-/-) were previously described.(*4*) Tg*SNCA*(+/+)*Snca* -/- mice were crossed with *Snca* +/- mice to create first generation (F1) siblings that express Tg*SNCA*(+/-) on the *Snca-/-* or *Snca* +/- background (**Fig. S1A**). Our previous findings have shown that a single gene of *Snca*(+/-) in mice is able to reconstitute protection from WNV infection.(*2*) We challenged F1 siblings with West Nile virus (WNV, 1000plaque forming units(pfu), subcutaneous injection) and followed mice for encephalitis symptoms. WNV-infected Tg*SNCA*(+/-)*Snca* -/- mice exhibited significantly increased mortality compared to Tg*SNCA*(+/-)*Snca* +/- mice while both strains exhibited similar weight loss (**Fig. S1B,C**). These results suggest that asyn interacts with species-specific host factors to inhibit virus infection since human *SNCA* expression in the mouse model did not reconstitute asyn-dependent inhibition of virus-induced disease while expression of murine *Snca* expression increased survival following virus challenge.

To define specific immune pathways that may be involved in asyn-dependent viral immune responses, we inoculated asyn wild-type (WT, *Snca* +/+) and asyn KO (*Snca* -/-) mice with mock diluent or WNV (1000pfu, subcutaneous inoculation). At day 8 post-infection, we harvested brain tissue and analyzed total RNA using RNAseq. While mock-inoculated WT and asyn KO mice exhibited similar gene expression profiles, we found that large sets of genes were upregulated following WNV infection in the brains of both WT and asyn KO mice (**Fig. 1A,B**). Principle component analysis revealed a clear subset of differentially regulated genes in WNV-

infected, WT brain tissue compared to WNV-infected asyn KO brain tissue (**Fig. 1C**). Specifically, a group of ISGs exhibited decreased expression in the brains of WNV-infected asyn KO mice compared to brain tissue from WNV-infected, WT mice. (**Fig. S2**)

To validate our RNAseq findings, we performed RT-qPCR on brain tissue from the same treatment groups. We found that gene expression of *Oas1b, Irf9, Tlr3, Trim25, and Tgtp1* were significantly more increased in the brains of WNV-infected, WT mice compared to brain tissue from WNV-infected, asyn KO mice (**Fig. 1D-H**). Notably, this was a subset of genes and there were many inflammatory pathway genes that were activated by WNV infection in both WT and KO mouse brain tissue (**Fig. 1I**). These data suggest that asyn KO mice are more susceptible to viral infection due to a deficient ISG response in the brain.

We next determined the cell types that might contribute to asyn-dependent ISG expression in the brain. Prior studies have demonstrated that asyn can be released by neurons and that asyn assemblies can activate microglia to promote an inflammatory response.(*5-7*), and some studies indicate this occurs through a TLR-dependent mechanism.(*6, 8-12*) Thus, we established a model to study acute central nervous system microglia activation following intracerebral inoculation of virus. We injected asyn WT and asyn KO mice by intracerebral inoculation with VEEV TC83 (TC83, 1000pfu). The TC83 virus is an attenuated virus due in part to a mutation in the 5' untranslated region that disrupts a stem-loop that is required to escape IFIT1 restriction.(*13*) Following intracerebral inoculation, TC83-infected asyn KO mice exhibited significantly increased weight loss compared to TC83-infected asyn WT mice (**Fig. 1A**). At day 4 post-infection, mice were sacrificed and plaque assay analysis revealed significantly increased TC83 virus titer in the brains of asyn KO mice compared to WT mice (**Fig. 1B**). We next determined the role of asyn in activation of microglia in the brain by

inoculating asyn WT and KO mice with TC83 (1000pfu, intracerebral injection) and harvested brain tissue at day 4 post-infection, a time point prior to significant peripheral inflammatory cell infiltration. Flow cytometry analysis of brain tissue revealed significantly increased numbers of CD45+CD11b+CD68+ cells, CD45+CD11b+IL6+ cells, and CD45+CD11b+TNFalpha+ following TC83 infection in both WT and asyn KO brain tissue, but we found no difference in CD45+CD11b+ cell activation when comparing asyn WT and KO brain tissue (**Fig. 2C-E, Fig. S3**). Histologic analysis for Iba1 and GFAP immunohistochemistry also provided evidence for microglia and astrocyte activation, respectively, in the brains of WNV-infected asyn KO and WT mice, without any significant differences between the two genotypes (**Fig. S4**). Next, we determined if microglial gene expression following virus infection in the brain was dependent on asyn expression. Using the same TC83 infection experimental model as above, microglia were column isolated from brain tissue using CD11b antibody binding. Total RNA was extracted from CD11b+ brain cells and analyzed by PCR array for ISG expression (**Fig. 2F**). ISG expression was normalized to mock-infected, WT microglia and revealed similar increases in ISGs following VEEV TC83 infection in both asyn WT and KO mice. Based on these data, we concluded that asyn-dependent regulation of innate immune responses and ISG responses were not due to differences in microglia activation following virus infection.

We next determined if the presence of asyn aggregates in the brain changes the microglial response to viral infection. We triggered the development of pS129 asyn pathology in WT mice by injection of exogenous asyn pre-formed fibrils (PFFs), or PBS as a control, into the right olfactory bulb followed by viral challenge using WNV (1000pfu, subcutaneous) 7 days later. We sacrificed mice at 14 days post-infection for histologic analysis. We found that WNV infection increased microglia activation, as measured by hydraulic radius of Iba1 expression ipsilateral to

the injection in the olfactory bulb, to an equal extent in both PBS- and PFF-injected mice (**Fig. S5**). These results indicate that the presence of pS129+ asyn pathology in olfactory pathway neurons does not affect acute activation of microglia during acute WNV infection when inoculated by a peripheral challenge of virus.

Next, we determined if dopaminergic neurons contribute to asyn-dependent ISG expression in the brain. Since neuron isolation from brain tissue alters gene expression patterns, we utilized CRISPR-mediated gene deletion of *SNCA* in human embryonic stem cells (hESCs) to create *SNCA* +/+ (WT), *SNCA* (-/+) and *SNCA* -/- (KO) engineered stem cells which were differentiated into human tyrosine hydroxylase+ (TH+) neurons as previously described (**Fig. 3A**).(*14*) Human asyn WT and asyn KO neurons were exposed to TC83 (MOI 1) and supernatant collected over 72 hours. We found that asyn KO neurons exhibited significantly increased TC83 viral titer compared to WT neurons (**Fig. 3B**). Next, we determined if loss of asyn expression altered ISG expression in human neurons following virus infection. Human asyn WT and asyn KO neurons were inoculated with TC83 (MOI 10), cells were harvested at 12 hours post-infection, and total RNA isolated. RT-qPCR analysis for gene expression for *IFIT1* and *TRIM25* expression revealed that asyn KO neurons exhibit significantly decreased gene expression of *IFIT1* compared to TC83-infected aysn WT neurons despite similar viral loads at this time point (**Fig. 3C**). Since *IFIT1* is an important restriction factor for VEEV TC83 and mutations in TC83 prevent *IFIT1* escape, then it follows that asyn KO neurons with decreased *IFIT1* expression would allow for increased viral growth as we have observed. Interestingly, TC83 did not significantly induce *TRIM25* in this human neuronal system such that no difference in *TRIM25* expression was noted between virus-infected WT and KO neurons (**Fig. 3D**).

Next, we determined if changes in ISG expression were related to RNA sensing mechanisms and type 1 interferon signaling. Asyn KO and WT neurons were treated with control diluent, Poly I:C, or type 1 interferon, and neurons were harvested at 4 hours post-treatment for RNA analysis using QPCR for *IFIT1* and *TRIM25* expression. Similar to our findings with TC83 virus, we found that asyn KO neurons exhibit significantly decreased gene expression of *IFIT1* following poly I:C treatment while *TRIM25* expression was not significantly induced in human neurons (**Fig. 3E,F**). However, we found significantly decreased expression of both *IFIT1* and *TRIM25* in asyn KO neurons compared to WT neurons following type 1 interferon treatment (**Fig. 3G,H**). These data show for the first time that asyn expression supports ISG expression in neurons following RNA virus infection, RNA sensing & signaling, and type 1 interferon stimulation. Since type 1 interferon is down-stream of poly I:C mediated activation of innate immune responses and asyn-dependent expression of TRIM25 occurs down stream of type 1 interferon stimulation but not poly I:C stimulation, we hypothesize that asyn interacts with type 1 interferon signaling pathways to support and regulate ISG expression in neurons.

Our data show that asyn-dependent ISG expression in neurons plays a role in the increased susceptibility to viral infection independent of microglia activation. Next, we determined the consequence of asyn-dependent ISG expression on adaptive immune responses during infection. Prior to initiation of our studies, we tested our backcrossed (F7 generations) asyn KO and WT colony and found 98% genetic similarity to C57BL/6 mice upon microsatellite analysis and completed a disease free morbidity analysis following WNV infection (1000pfu, subcutaneous inoculation). We found significantly decreased survival in virus-infected asyn KO mice compared to WT mice (**Fig. S6A**) but found no differences in total IgG and IgM responses

to viral infection in asyn WT and KO mice (**Fig. S6B,C**). Thus, we found no evidence that asyn expression alters total antibody responses during acute viral infection.

Prior studies have shown that asyn expression supports cytotoxic T-cell responses in Parkinson's Disease (PD) models.(*15-18*) Therefore, we evaluated T-cell responses in the brains of virus-infected WT and asyn KO mice using flow cytometry analysis (**Fig. S7**). WT and asyn KO mice were inoculated with mock diluent or WNV (1000pfu, subcutaneous), and brain tissue was collected at day 8 post-infection. Flow cytometry analysis of brain tissue revealed significantly increased CD3+ and CD4+ cells following WNV infection in both WT and asyn KO groups (**Fig. S8**). Since frequencies of T-cells were similar in the brain tissue of WNV-infected WT and asyn KO mice in the brain, we next evaluated specific activation markers for T-cell subsets. We found that WNV-infected asyn KO mice exhibited significantly decreased frequencies of CD8+CD25+ T-cells, CD4+IFNgamma+ T-cells, TNF+ NK cells, and IL2+ gd T-cells (**Fig. S9**). These data show that asyn-dependent ISG expression in neurons is important for activation of infiltrating anti-viral T-cell responses in the brain.

Since work has focused on RNA viral pathogens, we expanded our studies to investigate the role of asyn during an infection with a DNA virus, herpes simplex type 1 (HSV1). Asyn WT and asyn KO mice underwent eye excoriation and inoculation of HSV1 (1000pfu/microL). HSV1-infected asyn WT and KO mice exhibited similar symptom scores, similar number of facial lesions, exhibited no differences in HSV1 DNA and HSV1 RNA expression in the trigeminal ganglion, and exhibited no differences in HSV DNA viral loads in the brain (**Fig. S10**). This suggests that asyn-dependent immune responses do not restrict DNA viruses, such as HSV1.

Since alpha-herpesviruses are complex DNA viruses that are highly adapted to replicating in neurons, our results with HSV1 may be confounded by the efficiency of alpha-herpesvirus antagonism of the neuron-mediated innate immune response such that both WT and asyn KO mice exhibit similar phenotypes. To understand the interactions between RNA and DNA virus infection and asyn expression, we obtained pathologic tissue samples from infected neurons to determine if acute viral infections alter asyn expression.

We first determined if acute RNA virus infection causes accumulation of phosho-serine129 (pS129) asyn in human brain tissue. We evaluated histology from human brain tissue obtained at autopsy from patients with acute WNV encephalitis and found evidence of significantly increased levels of pS129+ asyn immunostaining in the grey matter of infected brain tissue compared to non-infected control brain tissue (**Fig. 4A-C**). Due to limited patient numbers, we were not able to comment on pS129 asyn expression levels for individual anatomical grey matter regions. Next, we evaluated histology of dorsal root ganglia from rhesus macaques after simian varicella virus (SVV), a DNA virus related to human varicella zoster virus, reactivation as previously described.(*19*) We found increased levels of pS129 asyn in dorsal root ganglion from SVV-infected rhesus macaques compared to seronegative control rhesus macaques (**Fig. 4D-F**). These data indicate that acute RNA and DNA virus infections induce increased levels of pS129 asyn expression in humans and rhesus macaques, respectively. More studies are needed to define the interactions between alpha-herpesvirus genes and asyn-dependent innate immune responses in neurons.

Asyn is known to localize to vesicle membranes during normal function and was shown to interact with several membrane proteins including Rab GTPases and SNARE proteins in the regulation of membrane vesicle functions.(*20-25*) Previously, we found that acute RNA virus

infection results in asyn localization to membrane structures in neurons.(*2*) We propose a model in which asyn is a neuron-specific modulator of RNA sensing and interferon responses. Since asyn is believed to play a role in the pathogenesis of PD, it will be important to define the interactions between innate immune sensing and interferon signaling in PD. Accumulating evidence indicates that specific triggers can upregulate expression and post-translational modifications of asyn (eg: phosphorylation, glycated, truncation).(*1, 3, 26*) These changes are believed to promote the formation of Lewy pathology, which is thought to be key to the development and progression of PD. We propose that specific innate immune triggers increase expression of asyn and failure to degrade up-regulated or modified asyn can increase the risk for PD. If fundamental innate immune interactions drive asyn misfolding and development of Lewy pathology, then inhibition of these interactions may provide a novel target for therapies that reduce the risk for PD developing in the first place, as a consequence of situations of heightened immune responses or even slow its progression once it has started.

References

1. C. M. Bantle *et al.*, Infection with mosquito-borne alphavirus induces selective loss of dopaminergic neurons, neuroinflammation and widespread protein aggregation. *NPJ Parkinsons Dis* **5**, 20 (2019).
2. E. L. Beatman *et al.*, Alpha-Synuclein Expression Restricts RNA Viral Infections in the Brain. *J Virol* **90**, 2767-2782 (2015).
3. E. Stolzenberg *et al.*, A Role for Neuronal Alpha-Synuclein in Gastrointestinal Immunity. *J Innate Immun*, (2017).
4. Y. M. Kuo *et al.*, Extensive enteric nervous system abnormalities in mice transgenic for artificial chromosomes containing Parkinson disease-associated alpha-synuclein gene mutations precede central nervous system changes. *Hum Mol Genet* **19**, 1633-1650 (2010).
5. A. S. Harms *et al.*, MHCII is required for alpha-synuclein-induced activation of microglia, CD4 T cell proliferation, and dopaminergic neurodegeneration. *J Neurosci* **33**, 9592-9600 (2013).

6. C. Roodveldt *et al.*, Preconditioning of microglia by alpha-synuclein strongly affects the response induced by toll-like receptor (TLR) stimulation. *PloS one* **8**, e79160 (2013).
7. J. Schapansky, J. D. Nardozzi, M. J. LaVoie, The complex relationships between microglia, alpha-synuclein, and LRRK2 in Parkinson's disease. *Neuroscience* **302**, 74-88 (2015).
8. D. Beraud *et al.*, Microglial activation and antioxidant responses induced by the Parkinson's disease protein alpha-synuclein. *J Neuroimmune Pharmacol* **8**, 94-117 (2013).
9. D. Beraud *et al.*, alpha-Synuclein Alters Toll-Like Receptor Expression. *Front Neurosci* **5**, 80 (2011).
10. I. F. Caplan, K. A. Maguire-Zeiss, Toll-Like Receptor 2 Signaling and Current Approaches for Therapeutic Modulation in Synucleinopathies. *Front Pharmacol* **9**, 417 (2018).
11. C. Roodveldt *et al.*, Glial innate immunity generated by non-aggregated alpha-synuclein in mouse: differences between wild-type and Parkinson's disease-linked mutants. *PloS one* **5**, e13481 (2010).
12. V. Sanchez-Guajardo, N. Tentillier, M. Romero-Ramos, The relation between alpha-synuclein and microglia in Parkinson's disease: Recent developments. *Neuroscience* **302**, 47-58 (2015).
13. J. M. Reynaud *et al.*, IFIT1 Differentially Interferes with Translation and Replication of Alphavirus Genomes and Promotes Induction of Type I Interferon. *PLoS Pathog* **11**, e1004863 (2015).
14. Y. Chen *et al.*, Engineering synucleinopathy-resistant human dopaminergic neurons by CRISPR-mediated deletion of the SNCA gene. *Eur J Neurosci* **49**, 510-524 (2019).
15. C. Cebrian *et al.*, MHC-I expression renders catecholaminergic neurons susceptible to T-cell-mediated degeneration. *Nat Commun* **5**, 3633 (2014).
16. G. T. Kannarkat, J. M. Boss, M. G. Tansey, The role of innate and adaptive immunity in Parkinson's disease. *J Parkinsons Dis* **3**, 493-514 (2013).
17. J. Seo *et al.*, Chronic Infiltration of T Lymphocytes into the Brain in a Non-human Primate Model of Parkinson's Disease. *Neuroscience* **431**, 73-85 (2020).
18. D. Sulzer *et al.*, T cells from patients with Parkinson's disease recognize alpha-synuclein peptides. *Nature* **546**, 656-661 (2017).
19. V. Traina-Dorge *et al.*, Simian Varicella Virus Is Present in Macrophages, Dendritic Cells, and T Cells in Lymph Nodes of Rhesus Macaques after Experimental Reactivation. *J Virol* **89**, 9817-9824 (2015).
20. J. Burre *et al.*, Alpha-synuclein promotes SNARE-complex assembly in vivo and in vitro. *Science* **329**, 1663-1667 (2010).
21. A. A. Cooper *et al.*, Alpha-synuclein blocks ER-Golgi traffic and Rab1 rescues neuron loss in Parkinson's models. *Science* **313**, 324-328 (2006).
22. D. F. Tardiff *et al.*, Yeast reveal a "druggable" Rsp5/Nedd4 network that ameliorates alpha-synuclein toxicity in neurons. *Science* **342**, 979-983 (2013).
23. N. Thayanidhi *et al.*, Alpha-synuclein delays endoplasmic reticulum (ER)-to-Golgi transport in mammalian cells by antagonizing ER/Golgi SNAREs. *Mol Biol Cell* **21**, 1850-1863 (2010).

24. J. Burre, M. Sharma, T. C. Sudhof, alpha-Synuclein assembles into higher-order multimers upon membrane binding to promote SNARE complex formation. *Proc Natl Acad Sci U S A* **111**, E4274-4283 (2014).
25. A. D. Gitler *et al.*, The Parkinson's disease protein alpha-synuclein disrupts cellular Rab homeostasis. *Proc Natl Acad Sci U S A* **105**, 145-150 (2008).
26. H. Vicente Miranda *et al.*, Glycation potentiates alpha-synuclein-associated neurodegeneration in synucleinopathies. *Brain* **140**, 1399-1419 (2017).

Acknowledgments: We thank Dr. Vicki Traina-Dorge who performed the SVV inoculation and collection of tissue samples for prior work and allowed us to utilize samples from prior studies. We thank Emily Schulz for her technical assistance in the asyn fibril injections. This work was supported by VA Merit Funding (I01BX003863) and DOD PRMRP funding (contract W81XWH-17-1-0183) to J.D.B. M.E.J., J.A.S., M.L.E.G and P.B. are supported by a grant from Farmer Family Foundation. Y.C. and T.K. were supported by funding from the UK Centre for Mammalian Synthetic Biology. **Author contributions:** A.M. completed RNAseq studies, brain gene expression studies, microglia isolations and gene expression, and histology/imaging analysis. B.M. completed all experiments with primary neurons, microglial flow cytometry, and completed all experiments with VEEV TC83. Y.C. and T.K. created *SNCA* gene deletion hESCs and human neurons and provided support for human neuronal experiments. M.E.J., J.A.S., M.L.E.G. and P.B. provided training, support, and analysis of brain tissue in experiments with injected fibrils. J.M. created and supplied PFFs. B.K.D. provided human brain tissue samples and guided human autopsy studies. R.M. provided primate ganglion samples for analysis from macaque SVV studies. J.D.B. designed the studies, guided and completed all data analysis, synthesized all data, and wrote the manuscript with input from all co-authors. **Competing interests**: The authors declare no competing interests. **Data and materials availability**: All materials are available upon reasonable request following materials transfer agreement. All data

is available in the main text or the supplementary materials, and all sequence data is available through NCBI.

Supplementary Materials:

Materials and Methods

Figures S1-S10

References

Fig. 1

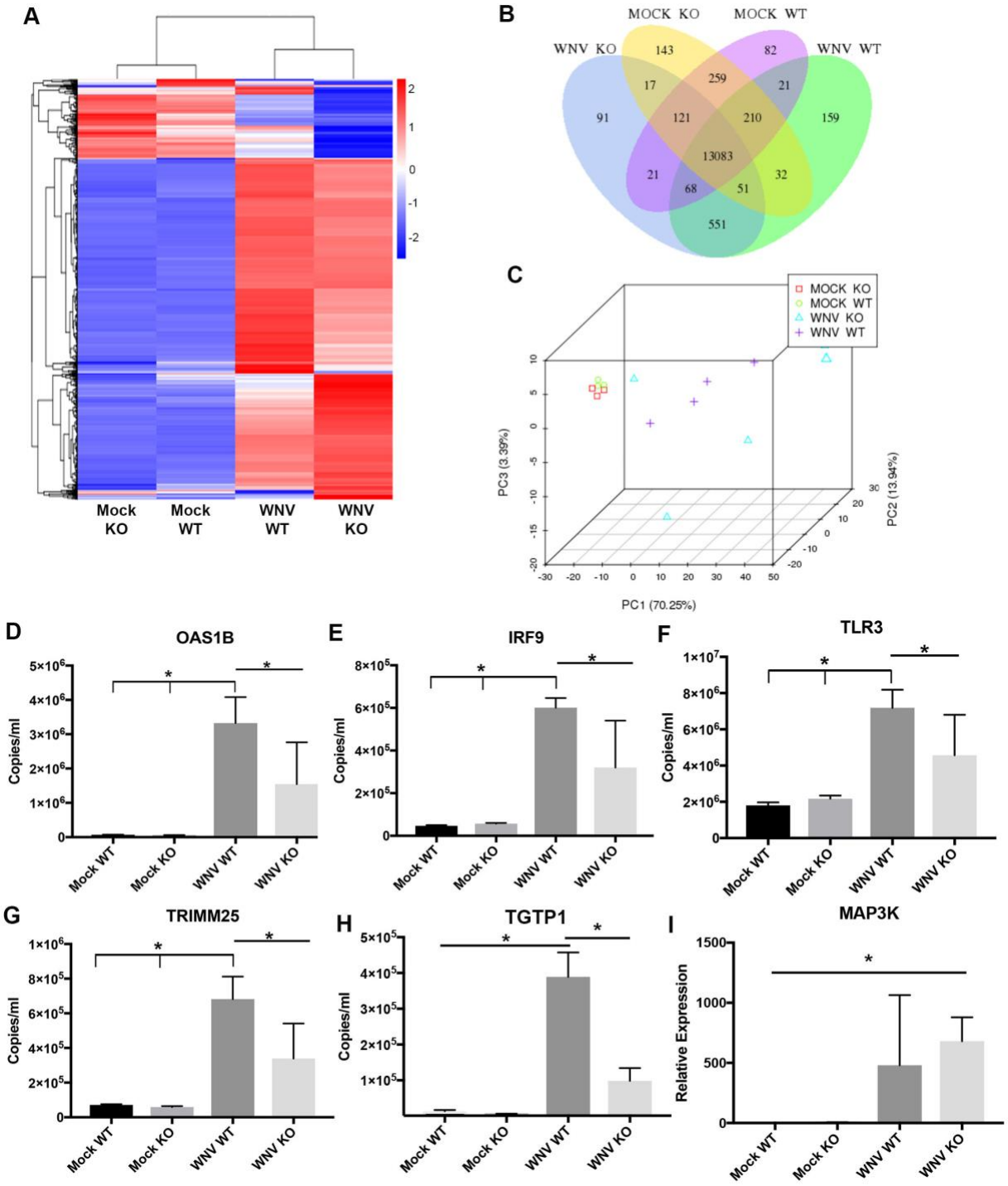

Fig. 1. Alpha-synuclein knockout mice exhibit decreased expression of specific ISGs in the brain following WNV infection. **A**) RNAseq heat map cluster analysis of differential expression of genes in the brain from indicated treatment groups using hierarchical clusters of

log10(FPKM+1). n=3 mice per group. **B**) Venn diagram of number of differentially expressed genes in each indicated treatment group and overlap between groups. **C**) Principal component analysis (PCA) using orthogonal transformation. QPCR values from brain tissue in indicated treatment groups to quantify expression of ISGs identified in RNAseq analysis including **D**) Oas1b, **E**) Irf9, **F**) Tlr3, **F**) Trim25, and **H**) TGTP1. **I**) Relative PCR expression compared to GAPDH for MAP3K in brains of mice. n=3 mice per treatment group. WT=asyn wild-type mice, KO=asyn knockout mice. *p<0.01. ANOVA.

Fig. 2.

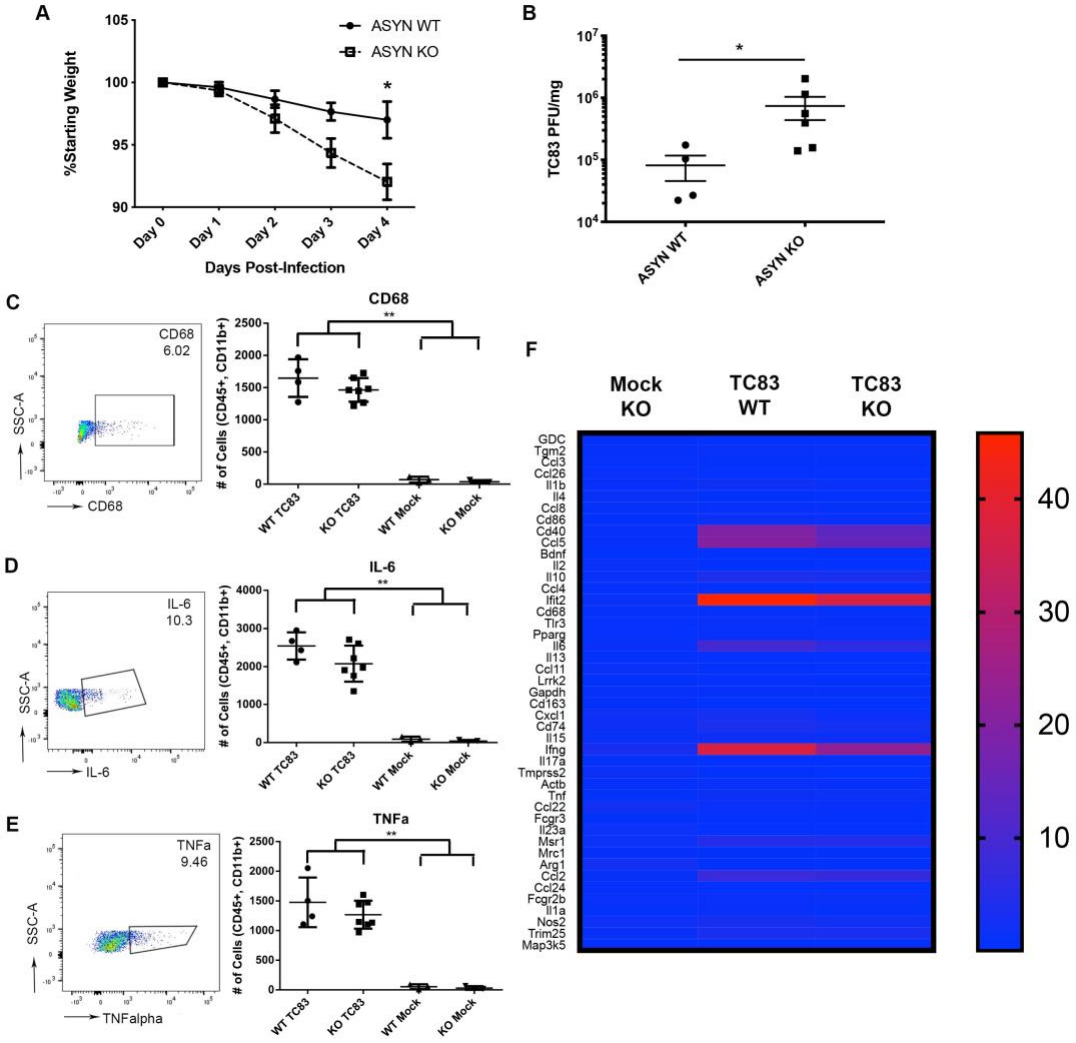

Fig. 2. Alpha-synuclein knockout mice exhibit no changes in microglial activation in the brain following acute viral infection. A) Asyn knockout (KO) and wild-type (WT) mice were inoculated with VEEV TC83 (10_5pfu, intracerebral inoculation) and followed for weight loss. *p<0.0001, Two-way ANOVA. N=6 mice per group. **B**) At 4 days post-infection with VEEV TC83, brain tissue from the indicated treatment groups was harvested and analyzed for VEEV TC83 titer using plaque assaya. *p=0.038. Mann-Whitney test. N=4-6 mice per group. Asyn KO and WT mice were challenged with TC83 or mock inoculum as above and multiparametric flow cytometry analysis was completed for CD45+CD11b+ cells in the brains of indicated treatment groups for **C**) CD68+, **D**) IL-6, and **E**) TNFalpha expression at day 4 post-infection. Each panel includes a representative flow plot, percent of cells expressing analyte, and a summary graph of flow cytometry data. **p<0.0001. ANOVA, n=4-7 mice per group. **F**) Following mock or VEEV TC83-inoculation by intracranial injection, microglia were isolated from brain tissue and analyzed for interferon stimulated gene expression using PCR array analysis. Data shown with a heat map representation of fold-increase in gene expression from isolated microglia compared to

wild-type (WT) mock-inoculated animals. WT=asyn wild-type mice, KO=asyn knockout mice. TC83=VEEV TC83 infection.

Fig. 3.

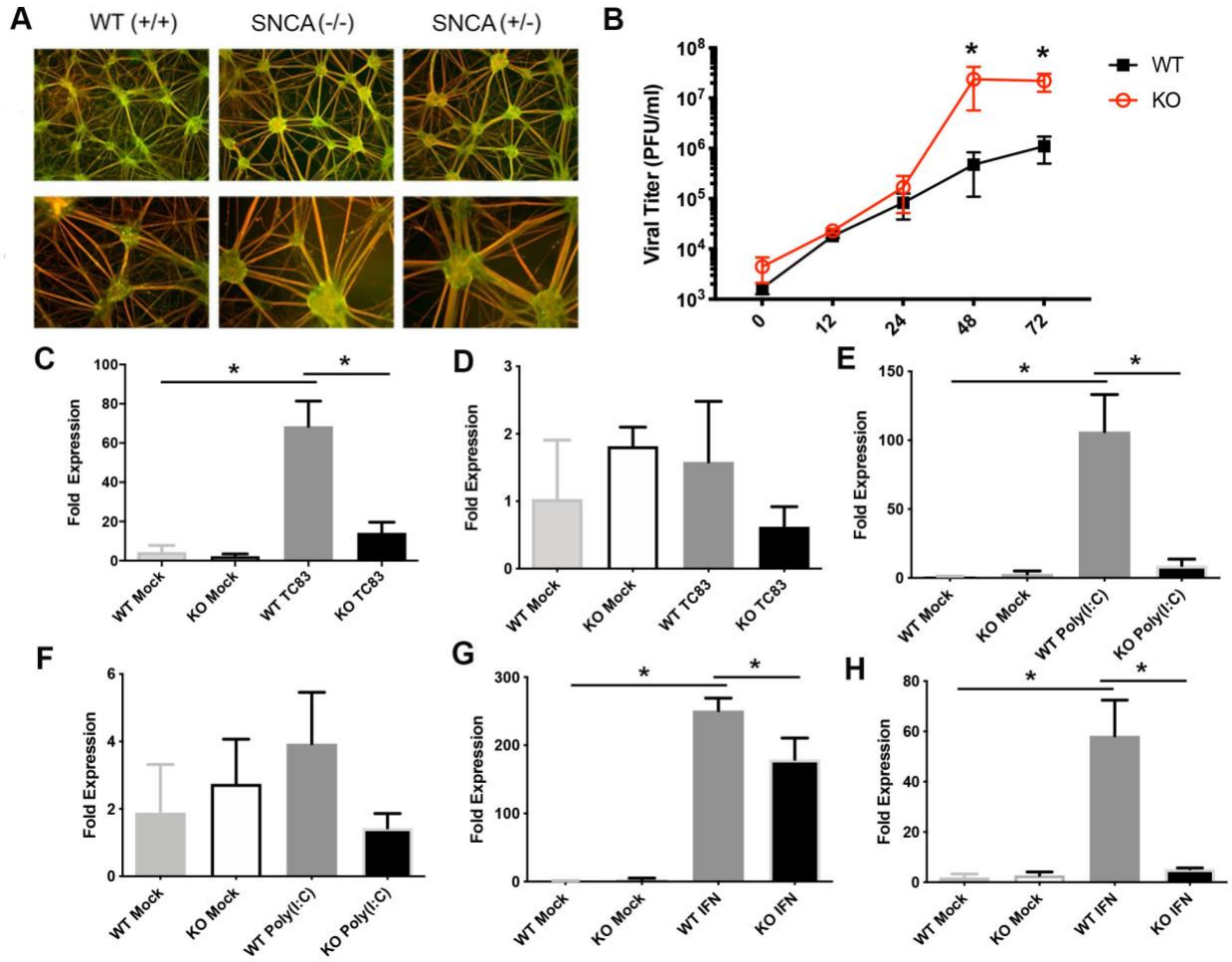

Fig. 3. Alpha-synuclein expression supports dsRNA sensing and signaling in primary neurons. **A**) CRISPR/Cas-induced knockout of one or two *SNCA* genes in embryonic stem cells (ESC) was completed followed by differentiation into primary human neurons positive for beta-III tubulin (red) and tyrosine hydroxylase (green). Images shown at day 42 in culture. **B**) Asyn WT and knockout (KO) neurons were inoculated with VEEV TC83 (MOI 1) and supernatant collected at indicated time points for viral titer assay. *p<0.05, two-way ANOVA, multiple comparisons. N=4 replicates per group. Next, asyn WT and KO neurons were inoculated with mock or VEEV TC83 (MOI 10) and neurons were harvested at 12 hours post-infection for gene expression analysis of **C**) IFIT1 and **D**)TRIM25 gene expression. *p<0.0001, One-way ANOVA, multiple comparisons. N=4-5 replicates per group. Asyn WT and KO neurons were treated with poly:IC (25 microg/ml) and neurons harvested at 4 hours post-treatment for **E**) IFIT1 **F**) TRIM25 gene expression analysis. N=3-4 per group. Asyn WT and KO neurons were treated with type 1 interferon (1000IU/ml) and cells harvested at 4 hours post-treatment for **G**) IFIT1 and **H**) TRIM25 gene expression analysis. *p=0.007, two-way ANOVA, multiple comparisons. N=3 per group.

Fig. 4.

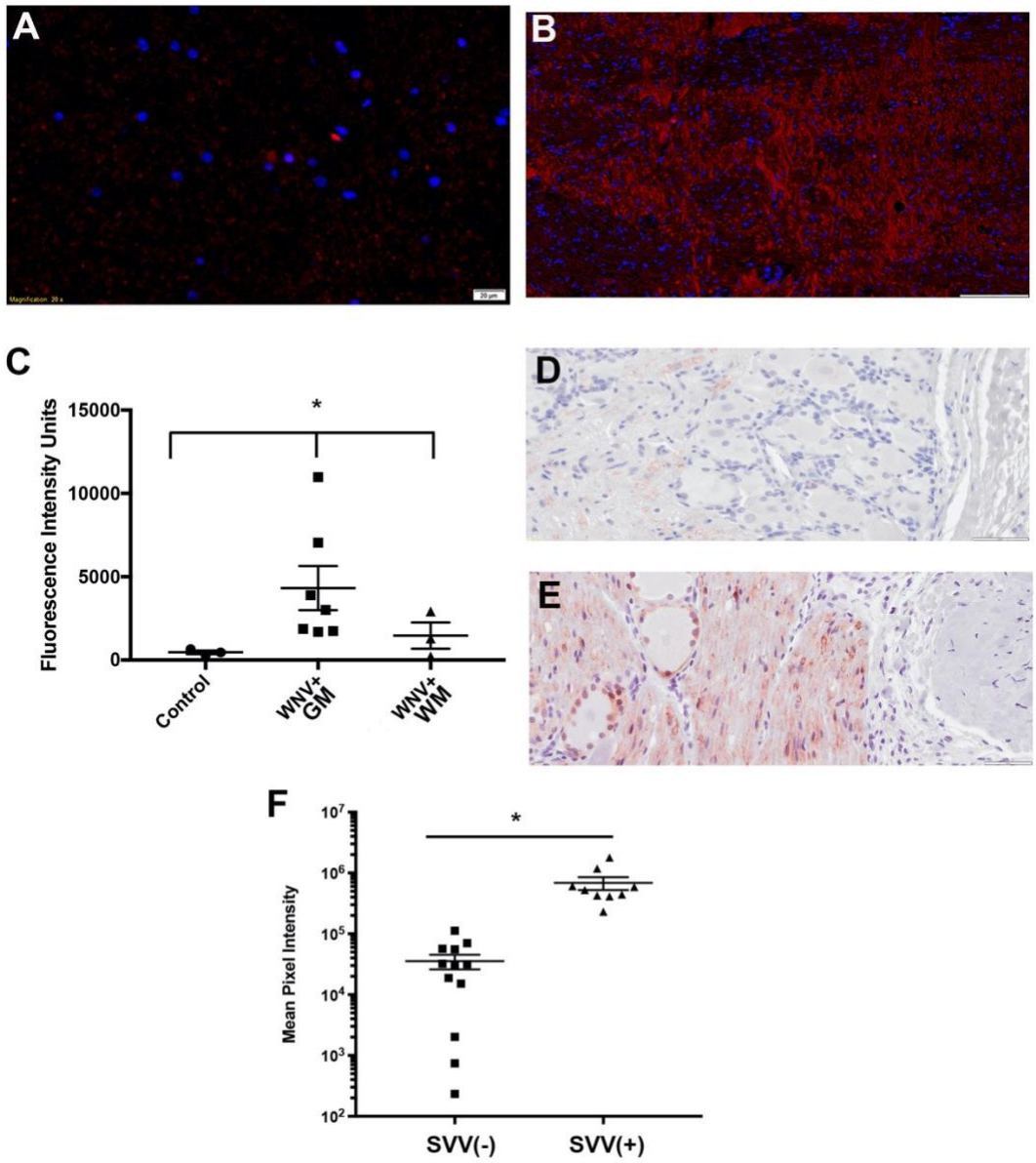

Fig. 4. Viral Infection of Human Brain and macaque ganglion results in accumulation of phospho-S129 alpha-synuclein. Immunofluorescent histology labeled tissue for phospho-S129 asyn (red) in **A**) uninfected control human midbrain tissue (bar=20microM). **B**) WNV-infected human pontine nucleus from a patient at day 10 hospitalization with acute encephalitis. Blue=DAPI stain, bar=50µm. **C**) Mean fluorescence intensity units per field of phopho-S129 asyn staining of human brain tissue acutely infected with West Nile virus (WNV). Each data point represents an individual patient in the indicated brain region. *$p<0.05$ ANOVA. GM=grey

matter, WM=white matter. Phospho-S129 asyn IHC (brown) of rhesus macaque lumbar dorsal sensory ganglion from **D)** simian varicella virus (SVV) seronegative control individual and **E**) SVV-reactivated rhesus macaque. Bar=50μm. **F**) Mean pixel intensity of phopho-S129 asyn measured per field from SVV-infected and uninfected rhesus macaque dorsal sensory ganglia. Each data point represents an independent section from 3 individual macaques per group. *p=0.0002, unpaired t-test.

Supplementary Materials for

Title: Alpha-synuclein expression supports interferon stimulated gene expression in neurons

Authors: Aaron R. Massey[1,6,8], Brendan Monogue[2,8], Yixi Chen[4], Kelsey Lesteberg[1], Michaela E. Johnson[5], Liza Bergkvist[5], Jennifer A. Steiner[5], Jiyan Ma[5], Ravi Mahalingam[3], Bette K. Kleinschmidt-Demasters[7], Martha Escobar Galvis[5], Patrik Brundin[5], Tilo Kunath[4], J. David Beckham[1,2,3,6*]

Affiliations:
[1] Division of Infectious Diseases, Department of Medicine, University of Colorado Anschutz Medical Campus, Aurora, CO.
[2] Department of Immunology&Microbiology, University of Colorado Anschutz Medical Campus, Aurora, CO.
[3] Department of Neurology, University of Colorado Anschutz Medical Campus, Aurora, CO.
[4] MRC Centre for Regenerative Medicine, School of Biological Sciences, and the UK Centre for Mammalian Synthetic Biology, University of Edinburgh, Edinburgh, UK
[5] Center for Neurodegenerartive Science, Van Andel Institute, Grand Rapids, MI
[6] Rocky Mountain Regional VA Medical Center, Aurora, CO
[7] Department of Pathology, University of Colorado Anschutz Medical Campus, Aurora, CO.
[8] These authors contributed equally.
*e-mail:David.beckham@cuanschutz.edu

This PDF file includes:

Materials and Methods
Figs. S1 to S10

Materials and Methods

Ethics statement

All animal work was performed at the University of Colorado Anschutz Medical Campus in accordance to and following approval by the Institutional Animal Care and Use Committee. All work with live viruses and recombinant DNA was approved by the University of Colorado Institutional Biosafety Committee and performed in accordance with local and national regulations of pathogens. Human brain tissue was obtained from de-identified human autopsies at the University of Colorado Hospital with approval for non-human research by the local Colorado Multiple Institutional Review Board. All work with hESCs was completed at the University of Edinburgh and ethics approval was granted by the MRC Steering Committee for the UK Stem Cell Bank and for the Use of Stem Cell Lines (ref. SCSC13-19). Differentiated neurons were provided to other laboratories for use following gene deletion and maturation. Support for hESC work was supported by grants through the Kunath laboratory.

Cell culture

All cell lines were maintained at 37°C in 5% CO2. Vero (ATCC CCL81) and BHK-21 cells were maintained in minimum essential medium containing Earle's salts and L-glutamine supplemented with 1% penicillin-streptomycin, 10% heat-inactivated fetal bovine serum, 1% nonessential amino acids, and 1% sodium pyruvate.

Snca$_{-/-}$ and *Snca*$_{+/+}$ human embryonic stem cells were generated and differentiated towards midbrain dopaminergic neuron for 16 by the Kunath laboratory as previously described.(*1*) Following this, the cells were frozen and shipped to the Beckham laboratory. Cells were then thawed and plated in L111-coated 48-well plates at a density of 800,000 cells/cm2.

Cells were differentiated for the following 26 days (42 days of total differentiation) in neuronal differentiation media consisting of Neurobasal Media (Thermo Fisher Scientific) + B27 supplement (without Vitamin A, 1:50, Thermo Fisher Scientific) + l-Glutamine (2 mM, Thermo Fisher Scientific) supplemented with ascorbic acid (AA, 0.2 mM, Sigma), brain-derived neurotrophic factor (BDNF, 20 ng/ml, Peprotech), glial cell line-derived neurotrophic factor (GDNF, 10 ng/ml, Peprotech), dibutyryl cyclic AMP (dcAMP, 0.5 mM, Sigma), and DAPT (1 μM, Tocris). Y27632 (Y2, 10 μM, Tocris) was present in medium from day 16 to day 17. Cellular media was removed and replaced every 3-4 days.

Virus propagation and quantification

West Nile virus strain 385-99 (NY99) was obtained from clone derived virus and propagated in *Aedes albopictus* (C6/36, ATCC CRL-1660) cells as previously described.(*2*) Venezuelan Equine Encephalitis virus (VEEV) TC83 isolates were obtained from the laboratory of Dr. Michael Diamond at Washington University in St. Louis and was propagated in BHK cells. Herpes Simplex virus type I (HSV-1) strain F was procured from ATCC (#VR733) and passaged over *Cercopithecus aethiops* kidney cells (Vero cells, ATCC CCL-81) at 34 $_{o}$C **.** Viral titers for all viruses were quantified in Vero cells by standard plaque assay as previously described.(*3*) Viral genome was quantified by probe-based qRT PCR.

The 3'UTR of WNV was amplified using forward primer CAG ACC ACG CTA CGG CG, reverse primer CTA GGG CCG CGT GGG, and probe /6FAM/TCT GCG GAG AGT GCA GTC TGC GAT/MGBNFQ/. The UL30 gene of HSV-1 was primed using forward primer CGC GTC CAA GCC CCG CAA, and reverse primer GGT GCC ACA CTT CGG GAA TAA ACC T, and quantified using probe /6FAM/ CCT CGG CCA GCT CGG ACA CCA /GMGBNFQ/. The nsP1 gene of VEEV TC83 was amplified using the forward primer GCC TGT ATG GGA AGC

CTT CA, reverse primer TCT GTC ACT TTG CAG CAC AAG AAT, and probe 6-FAM/ CCT CGC GGT /ZEN/ GCA TCG TAG CAG C/ 3IABkFQ/. Quantification was achieved by generating standard curves of serial diluted plasmids of known copy number and normalized to 18s rRNA copies. For 18s rRNA quantification, priming was achieved with the forward primer CGC CGC TAG AGG TGA AAT TC, reverse primer sequence CAT TCT TGG CAA ATG CTT TCG, and probe /6-FAM/CAA GAC GGA CCA GAG CGA AAG CAT/TAMRA/.

Mouse and Primate Studies

Snca$_{-/-}$ mice were obtained from Jackson Laboratories (#3692) and back-crossed seven generations to C57B/6J mice (#664). Microsatellite analysis performed by Jackson Laboratories confirmed mice were 96.3% C57B/6J. These mice were crossed with WT C57B/6J mice to generate *Snca*$_{+/-}$ heterozygous mice. Genotyping by conventional PCR was routinely performed to confirm *Snca* status as described.(*2*) Mice transgenic for human alpha-synuclein and deficient for murine alpha-synuclein (Tg*SNCA*$_{WT}$;*Snca*$_{-/-}$*)* were obtained from Jackson Laboratories (#10710) and crossed with mice heterozygous for murine alpha synuclein (*Snca*$_{+/-}$*)*. The offspring of these mice were tested via conventional PCR for the presence of both the human and murine alpha-synuclein genes to generate mice that had only the transgenic human alpha-synuclein (Tg*SNCA*$_{WT}$;*Snca*$_{-/-}$*)* and mice that had both the transgene and were heterozygous for murine alpha-synuclein (Tg*SNCA*$_{WT}$;*Snca*$_{+/-}$*)*. Virus used for infections was first diluted to the appropriate viral titer in HBSS before being administered by subcutaneous injection, intracranial injection, or corneal inoculation.

Prior to subcutaneous inoculation of virus, all mice were randomized, weighed, and placed under isoflurane-induced anesthesia. Equal numbers of male and female mice were used for all studies with the exception of the use of only female mice for the total brain RNAseq

analysis. For subcutaneous injections, 10 uL of virus solution was injected into the left footpad of mice with the use of a Hamilton syringe. For intracranial injections, 10 uL of virus solution was injected 3 mm deep into the brain near the Bregma with the use of a 25 gauge needle. Mice were monitored for morbidity and weighed daily. For HSV-1 inoculations, the corneas of anesthetized mice were scarred using a 31 gauge needle 9 times using a crosshatch pattern. Subsequently, 10^5 PFU HSV-1 was administered to the eye in 10 uL via pipette. Mice losing more than 15% bodyweight prior to the end of the study were euthanized and excluded from the study for humane reasons.

At the end of each experiment, mice were euthanized by isoflurane overdose before proceeding with tissue harvest. All mice were perfused with 20 mL of phosphate buffered saline solution (PBS) prior to tissue harvest. In the case of histology analysis, intracardiac perfusion of 4%PFA was completed. Samples collected for RNA gene expression assays, immunostaining assays, or viral quantification were collected and stored in RNALater (Invitrogen, #AM7021), 10% neutral buffered formalin (NBF), or PBS, respectively. Samples stored in RNALater and PBS were stored at -80 C until needed. Samples fixed in 10% NBF were stored at room temperature for 48 hours and subsequent storage at 4 ^{o}C in PBS until processed for paraffin embedding. Plasma was collected at time of euthanasia by cardiac stick, collected in EDTA coated microtubes. Blood cells were pelleted by centrifugation at 1500 rcf for 5 minutes at 4 ^{o}C, aliquoted and stored at -80 C until needed.

Unilateral injections of asyn fibrils into the olfactory bulb

Mouse α-synuclein amyloid aggregates were produced and kindly provided by Dr. Jiyan Ma, Van Andel Institute, USA. Before surgery, asyn fibrils were produced by the sonication of α-

synuclein amyloid aggregates in a water-bath sonicator for 10 min and were maintained at room temperature until injection. Mice were anesthetized with isoflurane and injected unilaterally in the right OB with either 0.8 µL of asyn fibrils (5 µg/µl) or 0.8 µL of PBS (phosphate buffered saline), as a control (coordinates from bregma: AP: + 5.4 mm; ML: - 0.75 mm and DV: - 1.0 mm from dura). Injections were made at a rate of 0.2 µL/min using a glass capillary attached to a 10 µL Hamilton syringe. After injection, the capillary was left in place for three min before being slowly removed. Prior to incision, the animals were injected with local anesthetic into the site of the future wound margin (0.03 mL of 0.5% Ropivacaine;
Henry Schein, USA). Following surgery mice received 0.5 mL saline s.c. for hydration.

Primate Studies

Simian varicella virus infection of non-human primates and collection of tissue samples were performed in the Tulane National Primate Research Center (TNPRC) in accordance with the recommendations of the US Department of Agriculture Animal Welfare Act regulations, the Guide for the Care and Use of Laboratory Animals, and the Institutional Animal Care and Use Committee (IACUC) at Tulane University and the TNPRC. The protocol for SVV infection and tissue analysis was approved ty the IACUC of Tulane University and the TNPRC.

Brain digestion and cell isolation

Cells collected from adult, infected mouse brain for flow cytometry were obtained as described.(*4*) Isolated cells were incubated overnight (5 hours for microglia analysis) in GolgiPlug and GolgiStop (BD Bioscience #555029 and #554724) in RPMI media containing HEPES and 10% fetal bovine serum (FBS) prior to staining and analysis by flow cytometry. Microglia were isolated from adult mouse brain using the multi tissue dissociation kit 1 (Miltenyi Biotec #130-110-201), followed by CD11b microglia isolation kit (Miltenyi Biotec #130-093-

634) according to manufacturer's protocols. Isolated cells were immediately stored in TRK lysis buffer (Omega) containing 25 uL/mL beta mercaptoethanol. Cells were stored in lysis buffer at -80$_{o}$C prior to RNA extraction.

Flow cytometry

The following antibodies were used for extracellular flow cytometry: anti-mouse CD45 BV650 (clone 30-F11, Biolegend), anti-mouse/human CD11b APC-Cy7 (clone M1/70, Biolegend), anti-mouse CD11c PE-eFluor 610 (clone N418, eBioscience), anti-mouse CD103 BV711 (clone 2E7, Biolegend), anti-mouse Ly6C BV785 (clone HK1.4, Biolegend), anti-mouse CD14 BV605, anti-mouse CD19 BV605, anti-mouse γδ TCR BV421, anti-mouse CD25 BV650, anti-mouse CD8 BV711, anti-mouse CD4 PE-Cy5.5, anti-mouse NK1.1 PE-CF 594, anti-mouse CD68 PE-Cy7, and anti-mouse CD3 BV785 (clone 17A2, Biolegend). The following antibodies were used for intracellular flow cytometry: anti-mouse CD68 PE-Cy7 (clone FA-11, Biolegend), anti-mouse IL-17 APC, anti-mouse IL-2 APC-Cy7, anti-mouse TNFα PE-Cy7, anti-mouse TNFα BV421, , anti-mouse IFNγ PE, anti-mouse IFNγ AF700, anti-mouse TNFa AF700 (clone MP6-XT22, Biolegend), anti-mouse IL-6 APC (clone MP5-20F3, BD Pharmingen), and anti-mouse IL-12 (p40/p70) PE (clone C15.6, BD Biosciences). Ghost Violet 510 dye (Tonbo Biosciences) was used to assess viability.

For flow staining, single cell suspensions were washed in PBS, centrifuged at 500 rcf for 5 minutes, and briefly vortexed. Next, 10 µL of viability dye (0.1 µL dye + 10 uL FACS buffer per sample) was added to each sample, vortexed, and incubated at room temperature for 10 minutes. Next, 50 µL of extracellular antibodies prepared in FACS buffer were added directly to each sample, vortexed, and incubated at 4°C for 25 minutes. 210 µL of Cytofix/Cytoperm solution (BD Biosciences) per sample was then added to permeabilize the cells, followed by

vortexing and incubation for 20 minutes at 4°C. The cells were then washed in 1 mL of 1x Perm/Wash buffer (BD) or Flow Cytometry Perm Buffer (Tonbo Biosciences) twice, centrifuged at 700 rcf for 5 minutes, and vortexed. Next, 50 µL of intracellular antibodies in Perm/Wash or Perm buffer were added to each sample, vortexed, and incubated at 4°C of 45 minutes. The samples were then washed once more in Perm/Wash buffer, centrifuged at 700 rcf for 5 minutes, vortexed, and finally fixed in 1% paraformaldehyde (Thermo Fisher).

The data was acquired on a LSRII flow cytometer (BD) using voltages standardized according to previously published methods (*5*). FlowJo software (FlowJo, LLC, Ashland, Oregon) was used to analyze the data. The gating strategies used are shown for individual experiments in the supplemental figures.

Cell Culture

Snca$_{-/-}$ and *Snca*$_{+/+}$ hESC derived midbrain dopaminergic neurons were grown as described above. Following this, the cellular media was removed and replaced with complete neuronal differentiation media (described above) containing VEEV-TC83 virus at a multiplicity of infection (MOI) of 1. 300 ul of the media was removed and replaced with fresh, virus-free neuronal differentiation media every 12 hours for 72 hours. The viral content of these samples was then titered via plaque assay as described previously(*2*). Differentiated neurons were infected with VEEV-TC83 at an MOI of 10. 12 hours post-infection, RNA from these cells was extracted and analyzed via qPCR (described below). Differentiated human primary neurons were treated with 10,000 IU/mL of mixed-type human IFNa, 25µg/mL of Poly(I:C), or mock treated. RNA from these cells was extracted 4 hours post-treatment and analyzed via qPCR.

Gene expression assays

RNAs collected from tissue were extracted using Trizol-chloroform extraction followed by column based isolation using the E.Z.N.A Total RNA kit II (Omega Bio-Tek #R6934) according to manufacturer's protocol. RNAs collected from cells were extracted using E.Z.N.A Total RNA kit I (Omega Bio-Tek #R6834) according to manufacturer's protocol. Qiagen's RT_2 custom PCR array was used to assay isolated microglia and neurons from infected mouse brain for interferon stimulated genes and microglia activation markers. RNA extraction and purification, cDNA synthesis, and Qiagen RT_2 custom PCR array was performed according to manufacturer's protocol and recommendations.

BioRad's PrimePCR probe-based qPCR assays for Oas1b, IRF9, TLR3, Trim25, TGTP1, and MAP3K were used to verify RNAseq results. RNA extraction, cDNA synthesis, and qPCR was performed according to manufacturer's protocols and recommendations. Normalization was achieved using 18s rRNA copy number as described above. BioRad's PrimePCR SYBR Green-based qPCR assays for Oas, TLR3, Trim25, and IFIT1 were used to analyze gene expression during infection and sterile immune-pathway activator treatment of differentiated $Snca^{-/-}$ and $Snca^{+/+}$ hESC derived neurons. RNA extraction, cDNA synthesis, and qPCR were performed according to manufacturer's protocols and recommendations. Normalization was achieved by calculating the ΔCT value of each sample compared to expression of the housekeeping gene GAPDH. Relative expression was calculated by comparing the ΔCT value of each sample to the average ΔCT value of the mock infected, WT mouse samples.

RNAseq analysis was performed on bulk brain RNAs by Novogene (Sacramento, CA, USA). Analysis of sequencing reads completed by Novogene and additional analysis of Fastq files completed in the Beckham laboratory. Following total RNA quantification (Nanodrop) from

brain tissue, we completed mRNA enrichment(poly-T oligo-attached magnetic beads), cDNA synthesis, end repair, poly-A and adaptor addition, fragment selection and PCR, and library quality assessment (Agilent2100) followed by Illumina sequencing (NovaSeq). Following data clean up, clean reads representing 96.51% of total reads were available for analysis at approximately 60-80million reads per sample. Mouse genome sequence alignment was completed with STAR with 85.7% of reads mapping to exons and fragments per kilobase of transcript sequence per millions base pairs sequenced (FPKM) calculated for gene expression. Overall gene expression was analyzed using principal component analysis and DESeq2 R package for differential expression analysis. ClusterProfiler software was used for enrichment analysis including GO enrichment, DO enrichment, KEGG and Reactome database enrichment.

Immunostaining assays

Five μm thick sections from formalin-fixed, paraffin-embedded tissue was used for immunostaining assays. The following primary antibodies were used; rabbit monoclonal antibody to serine 129 phosphorylated α-synuclein (1:200, Cell Signaling Technologies #23706), guinea pig antiserum to Iba-1 (1:100, SySY #234-004), chicken polyclonal antibody to GFAP (1:50, Abcam #ab4674), rabbit polyclonal antibody to WNV envelope protein (1:800, Novus Biologicals #NB100-56744), and rabbit polyclonal antibody to Iba-1 (1:200, Wako 019-19741). For immunohistochemistry, rabbit primary antibodies were detected with ImmPRESS HRP anti-rabbit IgG polymer detection kit (MP-7401) and ImmPACT NovaRED peroxidase substrate kit (SK-4805) according to manufacturer's protocol. For immunofluorescence the following detection antibodies were used; Cy5-conjugated goat anti rabbit IgG (1:200, Jackson ImmunoResearch #111-175-144), TRITC-conjugated goat anti chicken IgY (1:200, Jackson ImmunoResearch #103-025-155), and FITC-conjugated goat anti guinea pig IgG (1:200,

Rockland #106-102-002). Images were acquired using an Olympus VS120 slide scanning microscope and analyzed using ImageJ.

For the WNV study combined with asyn fibrils, 40 micron free-floating brain sections were incubated with 3% H_2O_2 for 20 min to quench endogenous peroxidase activity, blocked for 1 h with 5% normal goat serum and 0.3% Triton X-100, then incubated overnight at room temperature with Iba1 primary antibody (1:800, WAKO). Sections were incubated with goat anti-rabbit biotinylated secondary antibody (1:500, Vector Laboratories) followed by incubation with Avidin/Biotin ABC reagent (Vector Laboratories). Immunolabeling was revealed using diaminobenzidine, which yielded a brown-colored stain visible in bright-field light microscopy. Images were captured with a color Retiga Exi digital CCD camera (QImaging) using NIS Elements AR 4.00.08 software (Nikon) using the 60x magnification (oil immersion, 1.40 N.A.) on a Nikon Eclipse Ni-U microscope (Nikon). We assessed the morphology of microglia to determine to state of activation as activated microglia typically have a larger area:perimeter ratio. To do this we processed RGB color images using a custom MATLAB (Mathworks) script.

Immunoglobulin ELISAs

Total IgG and IgM from *Snca*$^{+/+}$ and *Snca*$^{-/-}$ were measured by commercially available ELISA kits (Invitrogen, #88-50400-22 and #88-50470-22) according to manufacturer's protocols. For WNV specific IgG, WNV particles were purified by ultracentrifugation over a 20% sucrose buffer, washed once and stored in PBS. Standard BCA assay was used to measure protein concentration (Pierce #23227). Two hundred and fifty ng whole WNV particles were plated in 100 uL of PBS into 96-well ELISA compatible microplates overnight at 4 ^{o}C. Plates were blocked in 5% BSA for 2 hours at room temperature before applying mouse plasma diluted

in PBS for one hour at 1 hour at room temperature. The mouse monoclonal pan-flavivirus antibody 4-G2 was used as a positive control and for generating standard curves. HRP-conjugated Donkey anti mouse IgG (1:600, Jackson ImmunoResearch #715-035-150) followed by TMB substrate were used for detection.

Statistical analysis

All statistical studies were completed using Gaphpad Prism software with the indicated statistical test in the text.

Methods References

1. Y. Chen *et al.*, Engineering synucleinopathy-resistant human dopaminergic neurons by CRISPR-mediated deletion of the SNCA gene. *Eur J Neurosci* **49**, 510-524 (2019).
2. E. L. Beatman *et al.*, Alpha-Synuclein Expression Restricts RNA Viral Infections in the Brain. *J Virol* **90**, 2767-2782 (2015).
3. E. Beatman *et al.*, West Nile virus growth is independent of autophagy activation. *Virology* **433**, 262-272 (2012).
4. C. Posel, K. Moller, J. Boltze, D. C. Wagner, G. Weise, Isolation and Flow Cytometric Analysis of Immune Cells from the Ischemic Mouse Brain. *J Vis Exp*, 53658 (2016).
5. S. P. Perfetto, D. Ambrozak, R. Nguyen, P. K. Chattopadhyay, M. Roederer, Quality assurance for polychromatic flow cytometry using a suite of calibration beads. *Nat Protoc* **7**, 2067-2079 (2012).

Fig. S1.

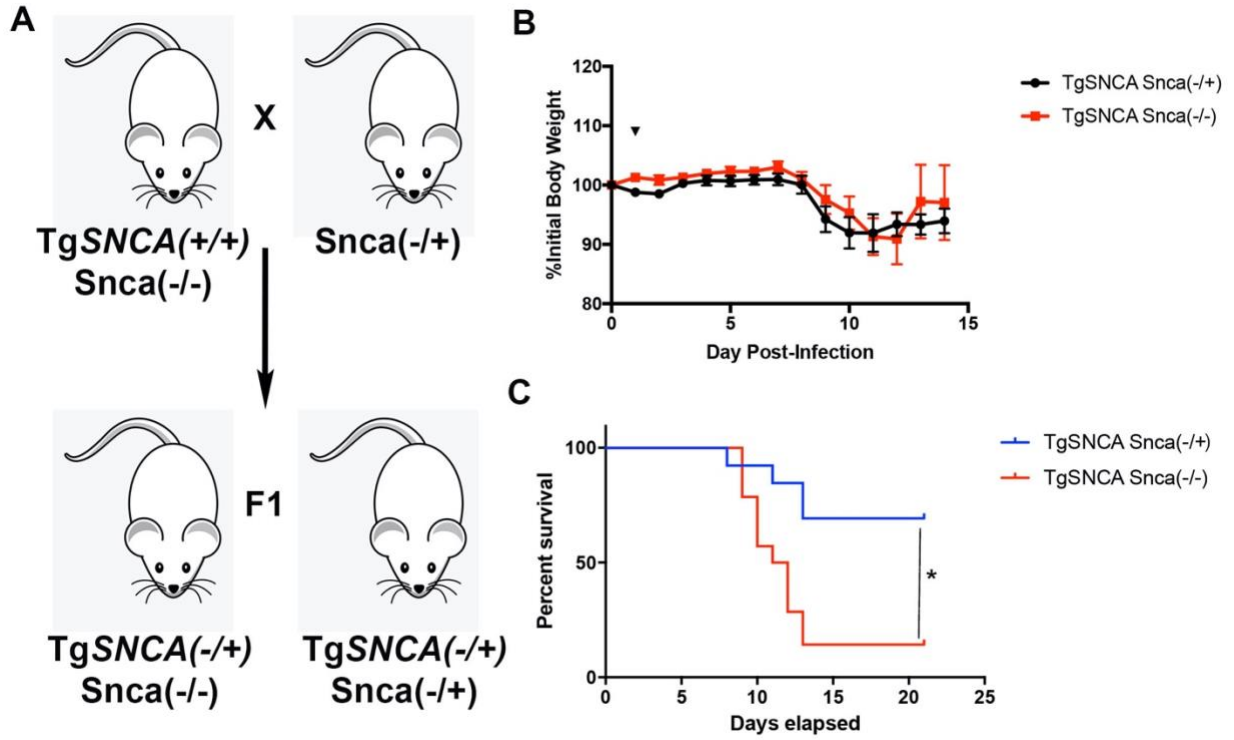

Fig. S1. Expression of human transgenic asyn does not protect mice from West Nile virus infection. A) Mice expressing human transgenic asyn (TgSNCA) on a murine asyn knockout background (Snca -/-) were crossed with mice heterozygotic for murine asyn (Snca -/+). F1 generation siblings expressing the human TgSNCA on a murine asyn KO (TgSNCA Snca(-/-), or mice expressing human TgSNCA on a murine asyn heterozygote background (TgSNCA Snca(-/+) were challenged with WNV (1000pfu, subcutaneous inoculation). **B**) Weight change following WNV inoculation in indicated treatment groups (n=9 per group). **C**) Following WNV challenge, mice in the indicated treatment groups were followed and sacrificed when moribund. *p=0.003 Log-rank test. N=7 per group.

Fig. S2.

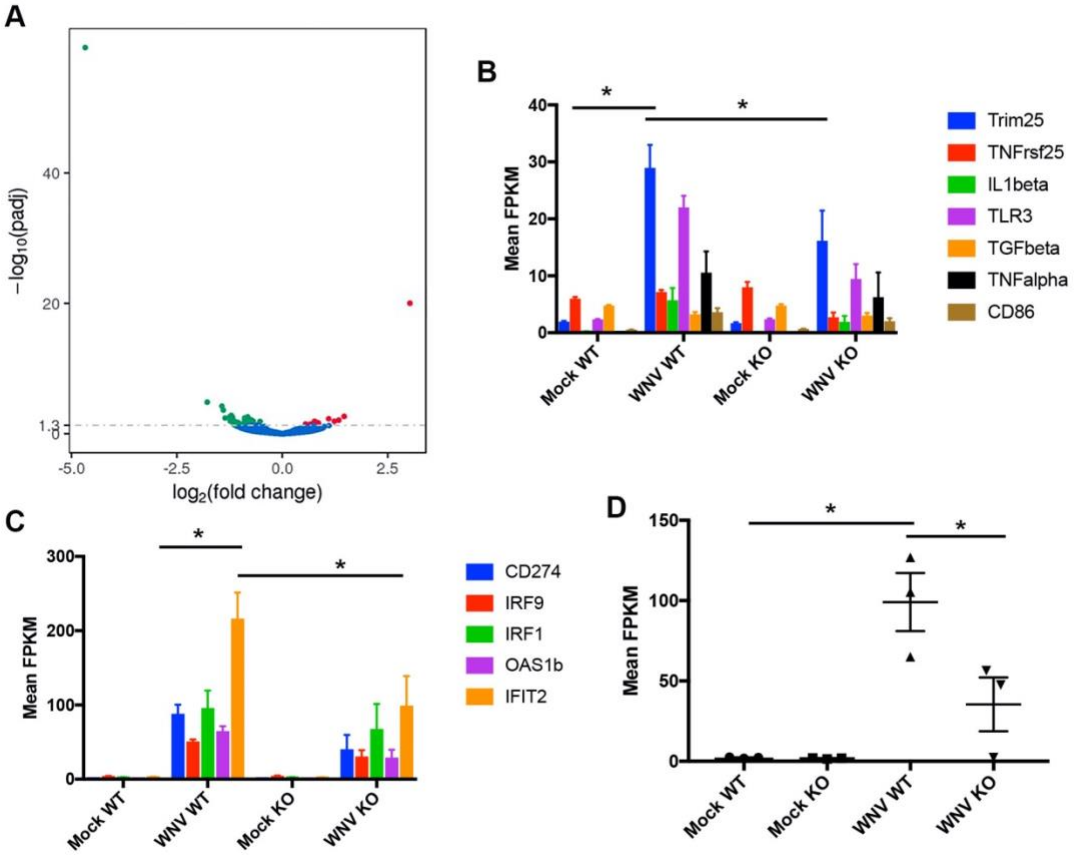

Fig. S2. Alpha-synuclein knockout mice exhibit decreased expression of specific interferon stimulated genes in the brain following infection. Asyn KO mice and wild-type control mice were inoculated with mock or WNV (1000pfu, subcutaneous inoculation) and sacrificed at day 8 post-infection and brain tissue analyzed using RNAseq. **A**) Volcano diagram showing fold change in WNV-infected asyn KO mouse brain tissue compared to WNV-infected wild-type mice with 13 genes up-regulated (red) and 39 genes down-regulated (green). Threshold $\log_2$ fold change >1.5 and p-value <0.005. n=4 mice per group. **B**) Graphical representation of mean FPKM values for selected interferon associated genes that were decreased in WNV-infected asyn KO mice compared to WNV-infected asyn WT mice. *p<0.0001, two-way ANOVA, n=3 per mock group, N=4 per WNV-infected group. **C**) Graphical representation of mean FPKM for selected interferon stimulated genes showing decreased gene expression as in A&B. *p<0.0001, Two-way ANOVA. **D**) Mean FPKM for *IRGM* expression. *p=0.0017, Two-way ANOVA. n=3 mice per group.

Fig. S3.

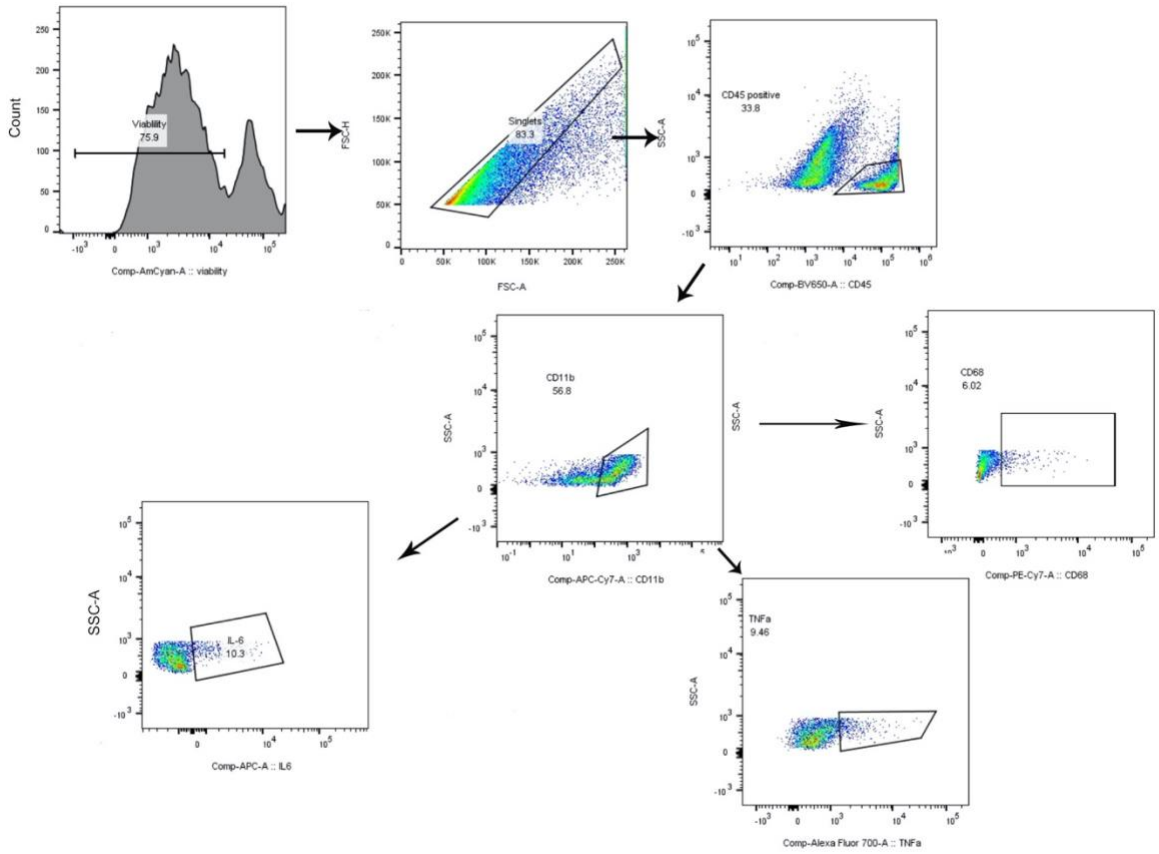

Fig. S3. Gating strategy for flow cytometry analysis of CD45+ cells in the brain. Cells were gated on viability and singlets were analyzed for CD45+ expression. Of the CD45+ cells, CD11b+ cells were analyzed for expression of CD68, TNFalpha, and IL-6.

Fig. S4.

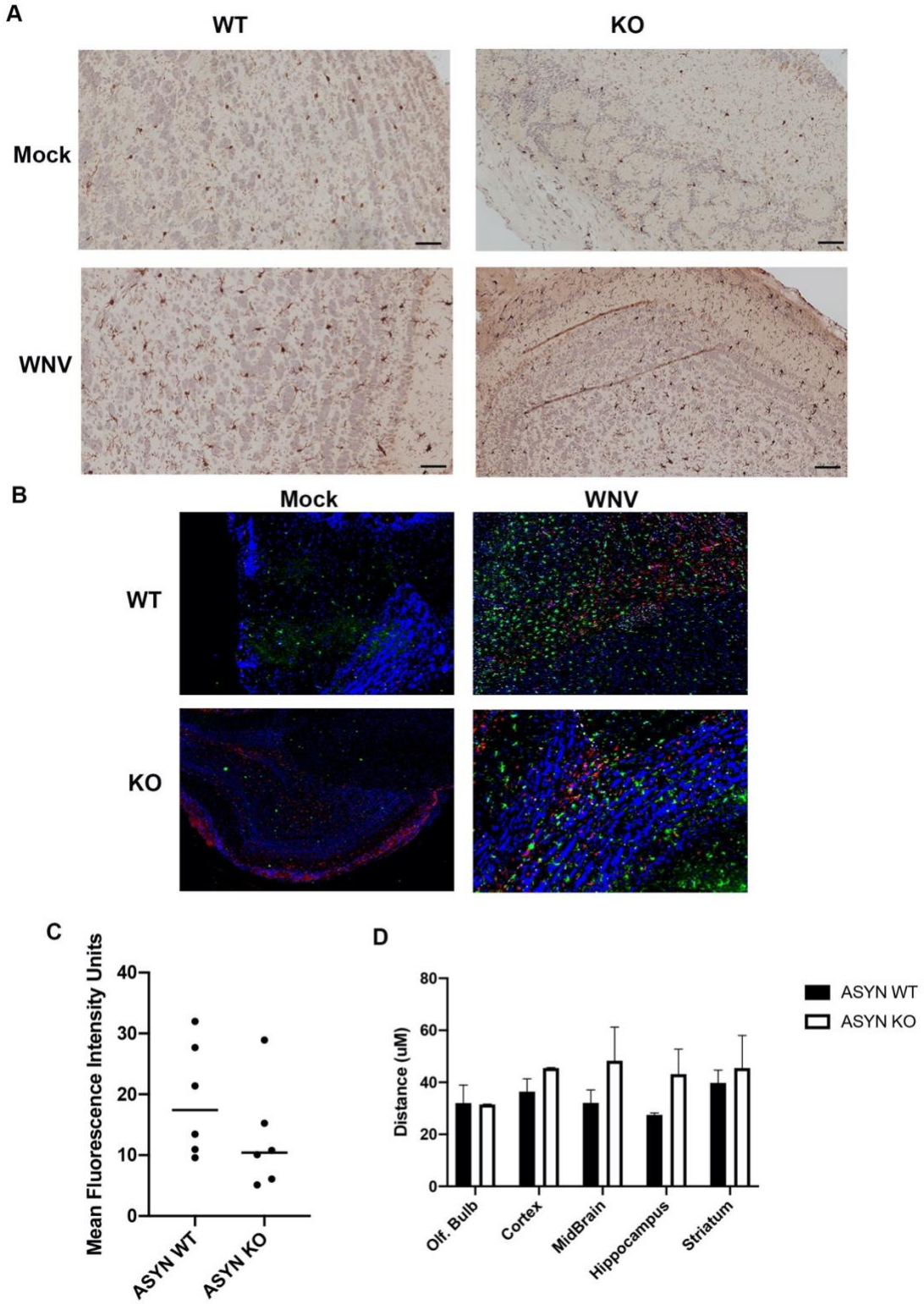
A
WT
KO
Mock
WNV
B
Mock
WNV
WT
KO
C
Mean Fluorescence Intensity Units
40
30
20
10
0
ASYN WT
ASYN KO
D
Distance (uM)
80
60
40
20
0
Olf. Bulb
Cortex
MidBrain
Hippocampus
Striatum
ASYN WT
ASYN KO

Fig. S4. West Nile virus increases microglia activation independent of ASYN expression. ASYN WT and KO mice were inoculated with WNV (1000pfu, subcutaneous inoculation) and brain tissue harvested for analysis at day 8 post-infection. **A**) Representative histology images of the cortex labeled with antibody to Iba1 in the indicated treatment groups indicates increased Iba1 staining following WNV infection in both ASYN WT and KO treatment groups. N=3. **B**) Immunofluorescence imaging from the same treatment groups showing representative images from the midbrain showing nuclei (DAPI, blue), microglia (Iba1, green), astrocytes (GFAP, red), and WNV envelope antigen (white) showing evidence of increased expression of Iba1 and GFAP following WNV infection in both treatment groups. N=3 **C**) Quantification of mean fluorescence intensity (MFI) units per high power field of GFAP expression following WNV infection in the indicated treatment groups. p=0.24. Mean MFI obtained from N=6 mice per group. **D**) In each brain sample, two-point distance measured from WNV antigen-infected neurons to Iba1+ microglia and mean distance provided per brain section for WNV-infected ASYN WT and KO mice. N=3 mice per group. p=0.488, Mixed effects model, multiple comparisons.

Fig. S5.

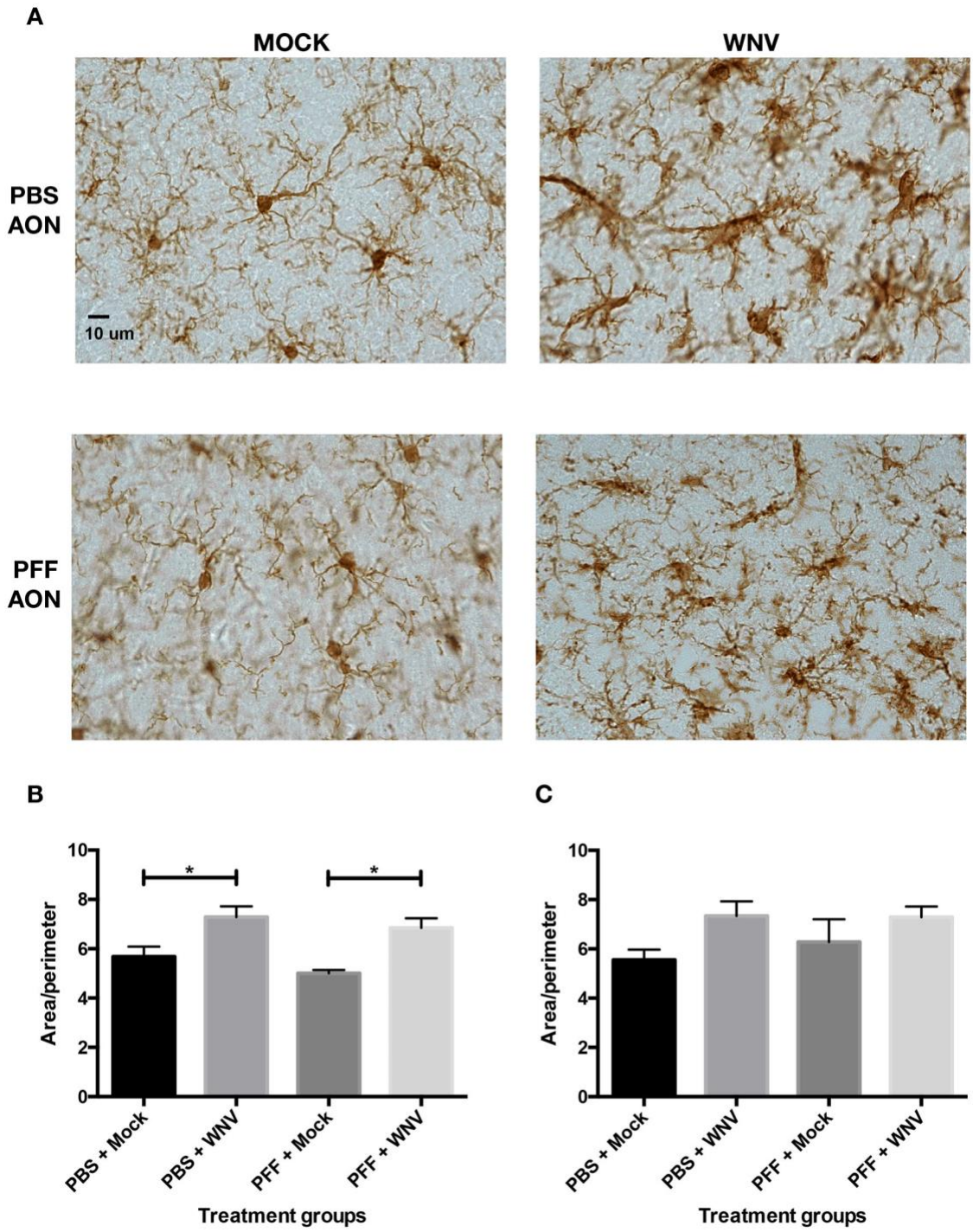

Fig. S5. West Nile virus infection increases microglia activation in the brain independent of pre-formed fibril (PFF) treatment. Histological sections of olfactory bulb (OB) were labeled with antisera to Iba1 in mock and WNV inoculated animals. C57B6 mice were inoculated with

PFFs or PBS in the right OB and 7 days later, mice were challenged with mock or WNV inoculation (1000PFU, subcutaneous). Brain tissue harvested at day 14 post-infection. **A)** Tissue from each treatment group was labeled with antibody to Iba1 followed by Matlab-guided area:perimeter analysis of microglia in the anterior olfactory nuclei, **B)** ipsilateral and **C)** contralateral to PFF injection. *$p<0.05$, ANOVA. AON=anterior olfactory nucleus.

Fig. S6.

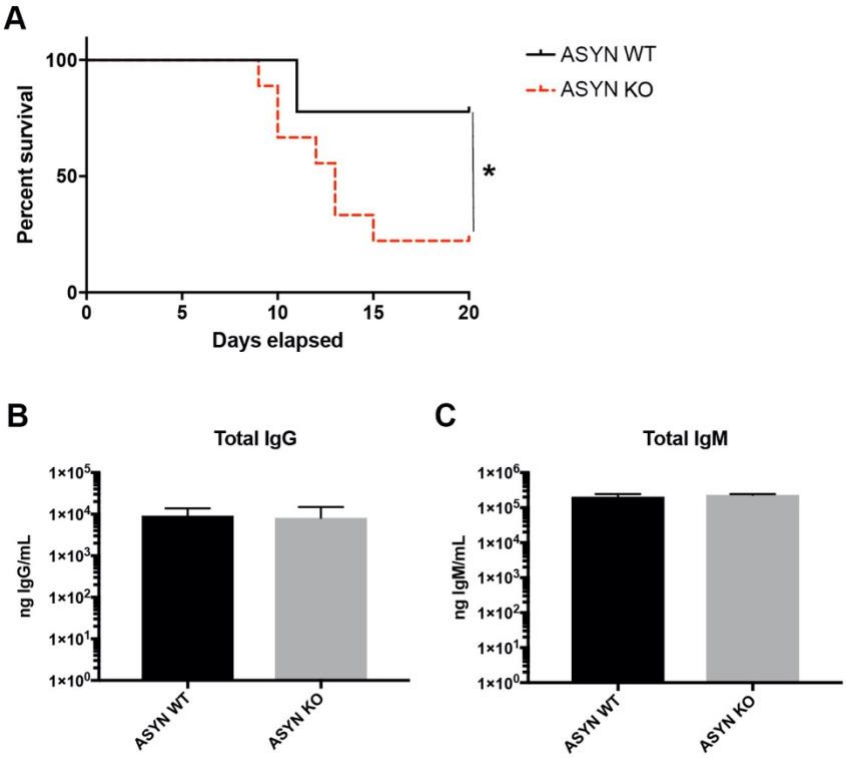

Fig. S6. West Nile virus infection causes increased mortality in asyn KO mice independent of antibody responses. Following backcross and microsatellite analysis to verify 98% C57B6 background, we inoculated ASYN KO and WT mice with WNV (1000pfu, subcutaneous inoculation) and evaluated mice for morbidity and antibody responses. **A**) WNV-infected ASYN KO mice exhibited significantly increased mortality compared to WT control mice. *p=0.0276, Log-rank test. N=6 per group. Next, ASYN WT and KO mice were sacrificed at day 8 post-infection and evaluated for WNV-specific **B**) IgG and **C**) IgM antibody responses using an ELISA.

Fig. S7.

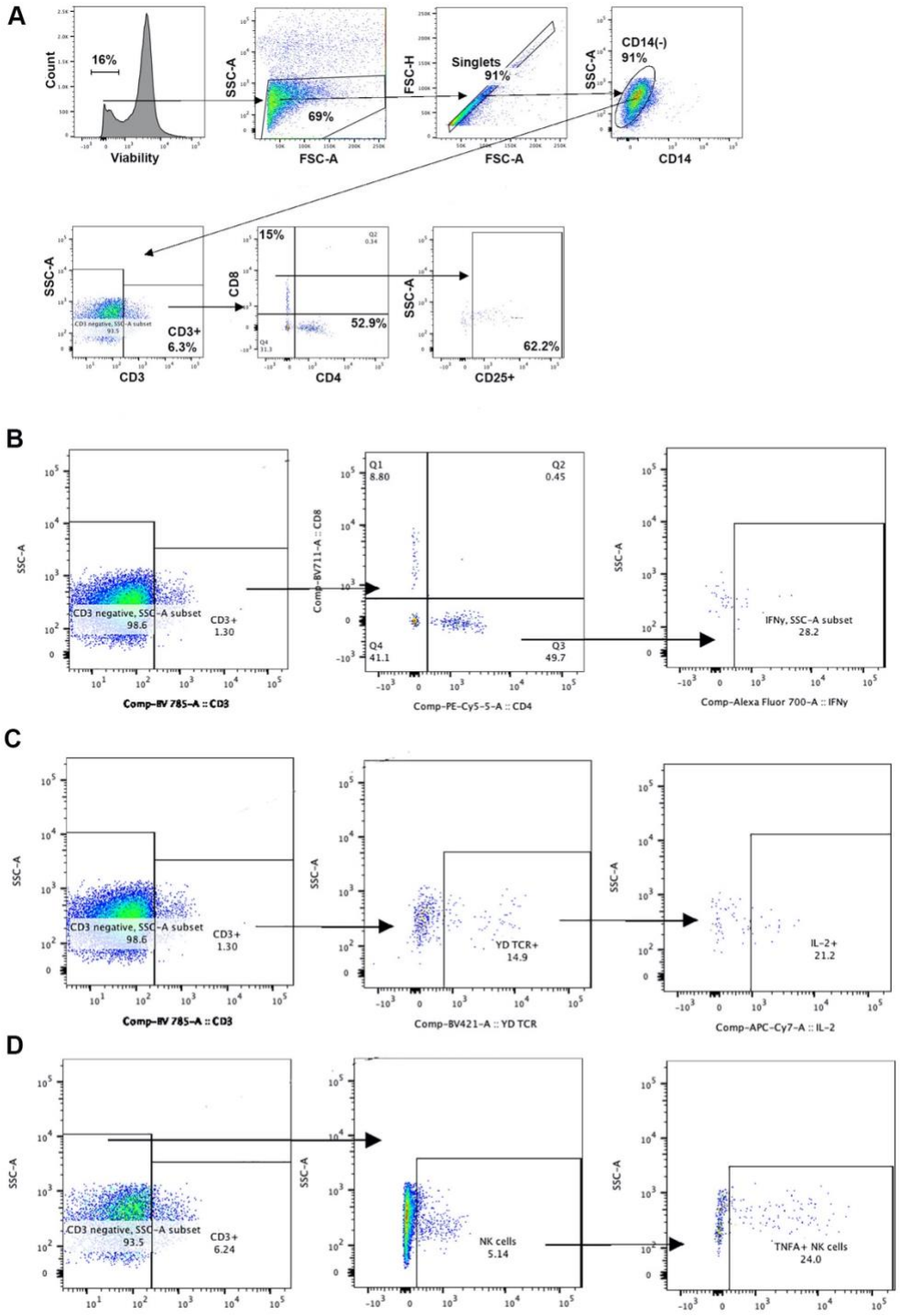

Fig. S7. Gating strategy for flow cytometry analysis of T-cells in the brain. Following viability selection, single cells were evaluated for CD14 expression. CD14- cells were analyzed for CD3 expression and CD3+ cells were gated for CD4+ or CD8+ expression followed by

determination of activation markers including **A**) CD25, **B**) CD4+, IFN-gamma, **C**) CD3+ γδTCR+ IL2+, **D**) CD3+ NK1.1+ TNFalpha+.

Fig. S8.

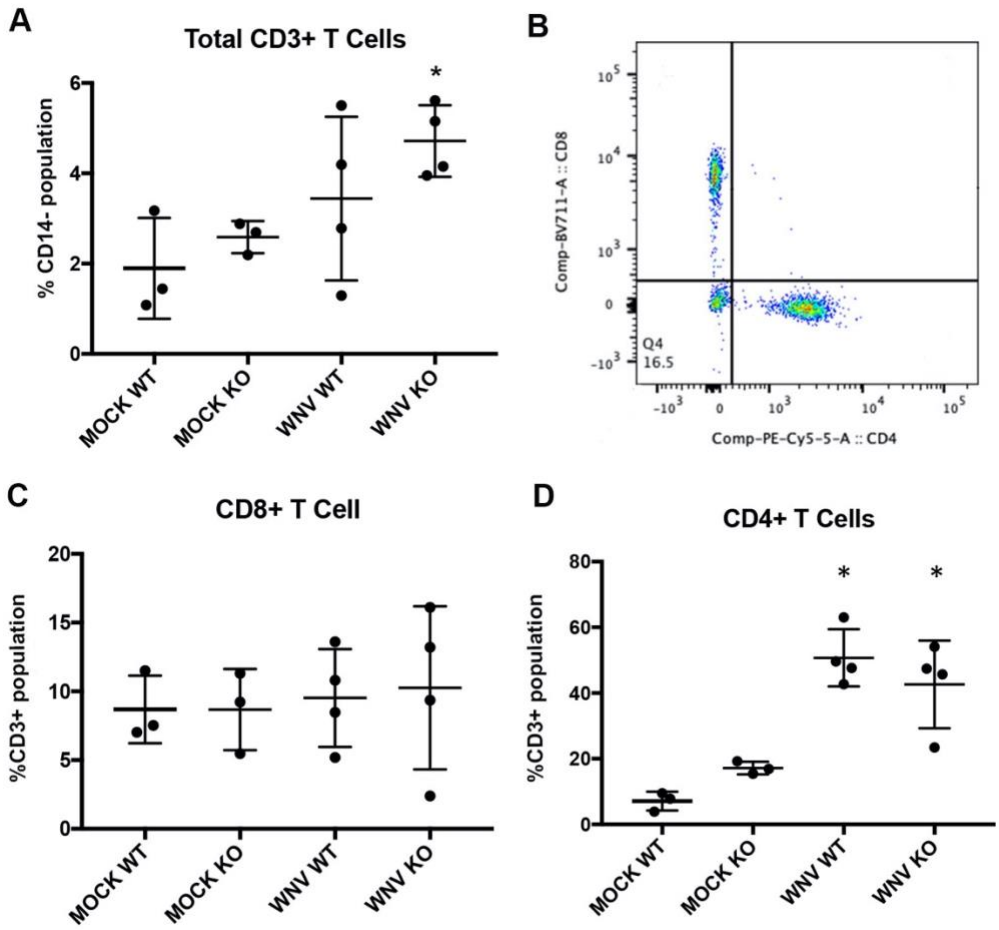

Fig. S8. Total T-cell counts increase in the brain following peripheral WNV infection. Mock and WNV inoculated (1000pfu) wild-type (WT) and ASYN KO (KO) mice were sacrificed at day 8 post-infection. Brain tissue was processed for multiparametric flow cytometry for activation markers of T cell subsets based on gating of CD14- cells. **A**) Following WNV infection, CD3+ cells were increased in WNV-infected mice. $p<0.05$. **B**) Representative gating of CD3+ cells into CD4+ and CD8+ cells following WNV infection in WT mice. **C**) The percentage of CD8+ cells did not significantly change in the brain following WNV infection. **D**) The percentage of CD4+ cells significantly increased following WNV infection in both ASYN WT and KO mouse brain tissue. *$p=0.01$. ANOVA.

Fig. S9.

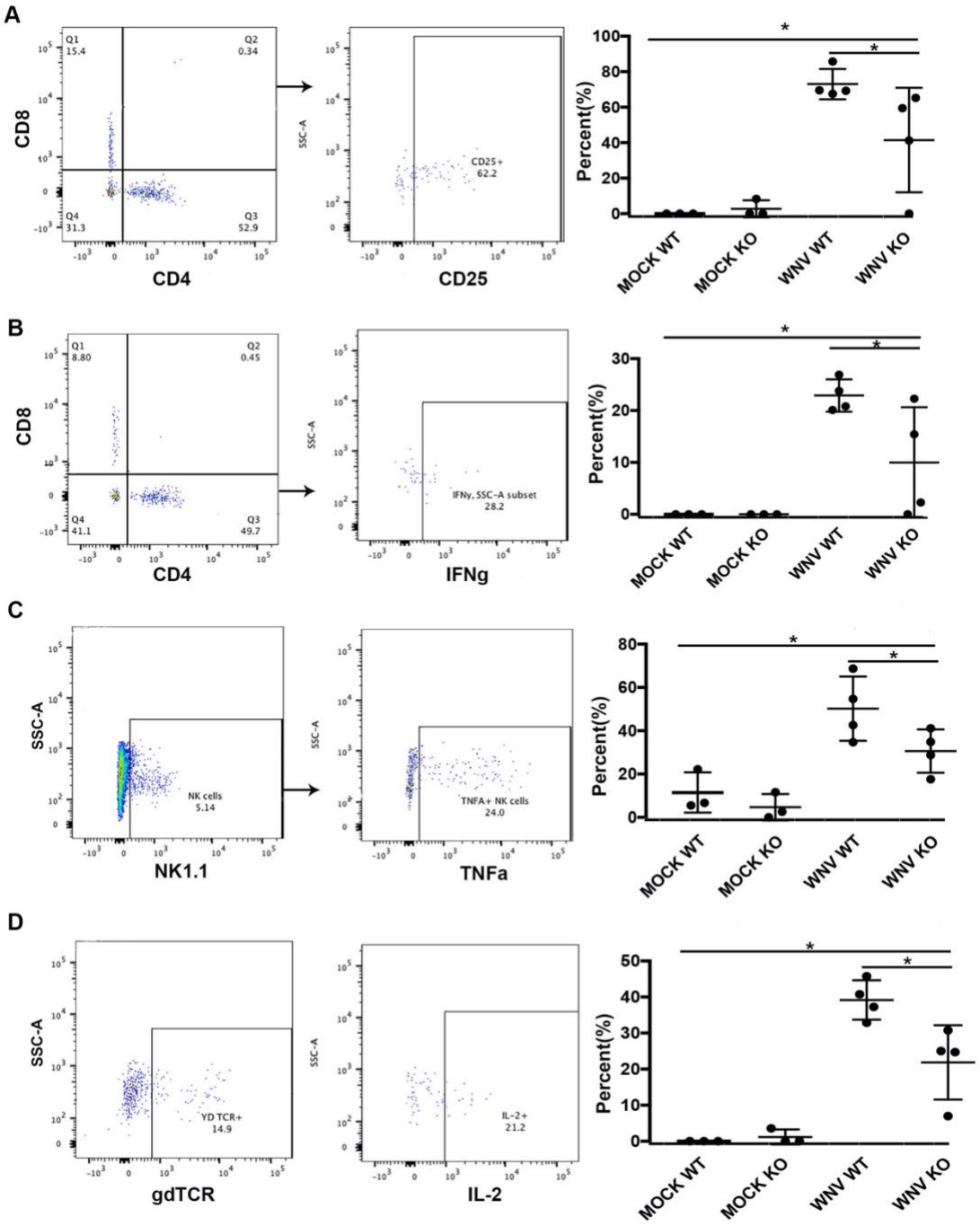

Fig. S9. Alpha-synuclein expression supports activation of T-cell effector function in the brain. Asyn WT and KO mice were challenged with mock infection or West Nile virus (WNV, 1000pfu) by subcutaneous footpad inoculation. At day 8 post-infection, animals were sacrificed, T-cells isolated and analyzed by flow cytometry for expression of **A**) CD25+ CD8+ cells, **B**) interferon-gamma+ CD4 T-cells, **C**) TNF-alpha+ NK cells, and **D**) IL2+ γδT-cells. *p=0.01. ANOVA, N=3-4 mice per group.

Fig. S10.

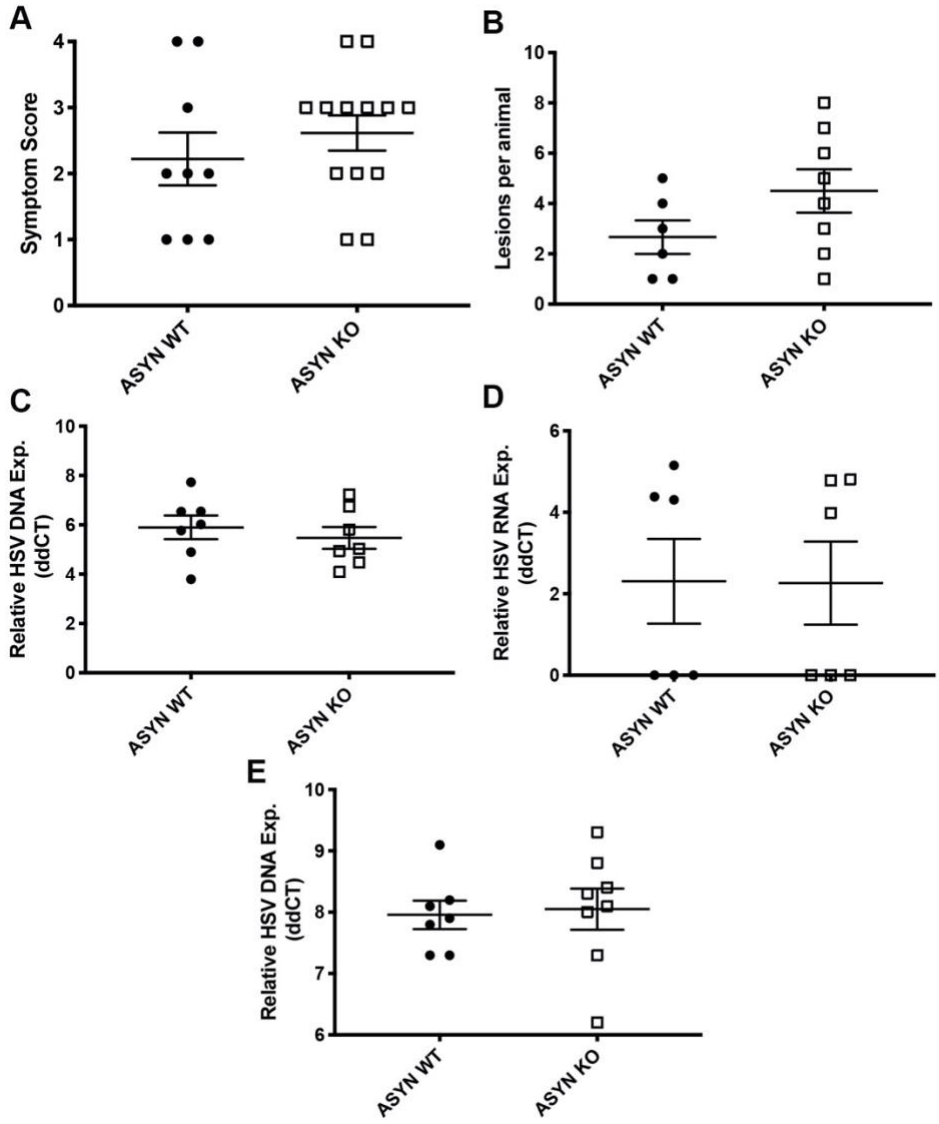

Fig. S10. ASYN expression has no effect on Herpes Simplex virus type I infection in the murine model of disease. ASYN WT and KO mice underwent eye excoriation and inoculation of Herpes Simplex virus type I (HSVI) by eye drop (1000pfu/microL). **A**) Following infection, symptom scores were completed on mice at day 8 post-infection on a scale of 0 (no disease) to 4 (encephalitis symptoms). N=9 mice per group. **B**) At day 8 post-infection, number of facial lesions was counted per animal. N=6-8mice per group. At day 8 post-infection, brain and trigeminal ganglia were isolated for PCR. Following HSV1 infection, there was no difference in **C**) trigeminal ganglion HSV1 DNA **D**) trigeminal ganglion HSV1 RNA, or **E**) brain HSV1 DNA expression in ASYN WT and KO mice.